J Solid State Electrochem (2008) 12:273–285
DOI 10.1007/s10008-007-0389-y

ORIGINAL PAPER

X-ray Photoelectron Spectroscopy and Time-Of-Flight Secondary Ion Mass Spectroscopy studies of electrodeposited molybdenum oxysulfide cathodes for lithium and lithium-ion microbatteries

V. Yufit · D. Golodnitsky · L. Burstein · M. Nathan · E. Peled

Received: 21 March 2007 / Revised: 5 July 2007 / Accepted: 10 July 2007 / Published online: 14 August 2007
© Springer-Verlag 2007

Abstract Thin-film molybdenum oxysulfide cathodes for lithium and lithium–ion microbatteries were fabricated by a simple electrodeposition method. According to Scanning Electron Microscopy (SEM) data, the deposition parameters affect the morphology of the cathodes. X-ray diffraction (XRD) tests indicated that the sub-micron-thick molybdenum oxysulfide films are amorphous or form too small crystallites to give rise to detectable X-ray diffraction peaks. A variety of poly-ion clusters containing both oxygen and sulfur (like MoOS, MoO_2S and MoS_2O and others) detected by TOF-SIMS tests unambiguously indicates the formation of molybdenum oxysulfide compounds, and not a mixture of oxides and sulfides, during electrodeposition. The sulfur-to-oxygen ratio in the bulk of the deposit is about 1.76 and does not depend much on the electrodeposition parameters. XPS studies reveal that electrodeposition in unbuffered solutions produces deposits with high oxygen and low sulfur content, as compared with cathodes deposited in buffered solutions. Potentiostatic, as compared to galvanostatic deposition, is followed by the formation of cathode films with slightly higher sulfur and lower oxygen content at the same pH. An increase in the pH of electrolyte solutions from 8 to 9.5 slightly reduces sulfur content, but appreciably increases oxygen concentration. Charge–discharge overpotential of Li/hybrid polymer electrolyte microbatteries is lower in sulfur-rich MoO_xS_y cathodes.

V. Yufit · M. Nathan
Department of Physical Electronics,
School of Electrical Engineering, Tel Aviv University,
Tel Aviv 69978, Israel

D. Golodnitsky · E. Peled
School of Chemistry, Tel Aviv University,
Tel Aviv 69978, Israel

D. Golodnitsky (✉) · L. Burstein
Wolfson Applied Materials Research Center, Tel Aviv University,
Tel Aviv 69978, Israel
e-mail: golod@post.tau.ac.il

Introduction

Recent progress of the Very Large Scale Integrated (VLSI) microelectronics has been made possible in three most essential processes: miniaturization, interconnection, and integration. However, the miniaturization of electronic components embodied by the present VLSI microelectronics technology has not been accompanied by a similar size reduction of power sources. Miniature power sources are needed for sustained mini- and micro-systems like Microelectromechanical systems (MEMS), smart cards, sensors, miniature radio frequency (RF) transmitters, microrobots, biochips, implantable medical devices, and other microdevices. Rechargeable, thin-film, lithium and lithium–ion microbatteries (MB) are potentially useful as power sources on integrated-circuit chips. Lithium and lithium–ion microbatteries can be fabricated in a variety of shapes. Due to their all-solid-state design, there is no worry about gaseous components generated during operation. Lithium and lithium–ion microbatteries feature long-cycle life, high energy and power densities. However, the capacity of such MBs is restricted by battery dimensions, and to date the best commercial planar or two-dimensional (2D) thin-film batteries have a reversible capacity of 0.133 mAh/cm^2 [1], which is quite small.

We have recently demonstrated the first working, three-dimensional, rechargeable microbattery (3DMB) that is compatible with microsystem on-chip-integrated power

requirements [2–5]. The technology has been developed for fabrication of 3DMB cells on both glass multichannel plates (MCP) and perforated silicon substrates. These substrates have thousands of high-aspect-ratio holes per square cm, thereby providing more than an order of magnitude increase in surface area per given footprint (original substrate area). The 3DMB cells that have been developed have a sandwich-like structure of conformal thin-film electrodes, electrolyte and current collectors. The complete 3DMB cell consists of a nickel current collector, a molybdenum oxysulfide cathode, a hybrid polymer electrolyte (HPE) based on PVDF-silica and a lithiated-graphite anode that also serves as an anode current collector. All available surfaces of a perforated substrate are coated sequentially by thin-film layers with the use of wet chemistry. For preparing low-cost and low-toxicity molybdenum oxysulfide thin cathode layers an inexpensive and relatively simple electrodeposition method has been proposed [6]. A highly adherent, homogeneous, compact molybdenum oxysulfide film about 300–500 nm in thickness can be deposited on nickel-coated silicon and glass substrates. The choice of molybdenum oxysulfide as a cathode in MBs was not accidental. The crystalline MoS_2 was firstly utilized as a cathode in primary lithium cells by Moli Energy in late 1980s. The reversibility of crystalline MoS_2 was found to be poor [7] however the amorphous molybdenum disulfide had demonstrated much better cycleability as a cathode in the lithium battery [8]. Thin amorphous MoS_2 films could be prepared by RF-sputtering [9] or CVD [10]. The CVD-deposited MoS_2 have demonstrated similar to amorphous molybdenum disulfide insertion/deinsertion behavior of lithium. The molybdenum trisulfide (MoS_3) cathodes can also be reversibly cycled. Although its specific energy is noticeably higher [11] than of MoS_2 its electrochemical behavior in Li cells has never been investigated. It is worth noting that MoS_3 can be also electrodeposited from aqueous solutions [12]. The molybdenum trioxide (MoO_3) and molybdenum dioxide (MoO_2) are well known for their ability to reversibly host lithium cations. The crystalline form of MoO_2 exhibits potential of 1.3 V vs Li and can be used as an anode [13], whereas crystalline MoO_3 demonstrates higher average potential of 2.5 V vs Li and can serve as a cathode [14]. None of these materials was ever commercialized in lithium cells. Molybdenum oxides can be easily electrodeposited from an aqueous solution of molybdate and used as cathodes in lithium cells [15]. The electrochemical characteristics of lithium or lithium ion battery with molybdenum-containing materials are strongly affected by chemical composition of sulfur or oxygen. Therefore, the current work places particular emphasis on morphological, structural and compositional characterization of thin electrodeposited free-of-binder molybdenum oxysulfide cathodes as a function of deposition parameters.

Experimental

Deposition was carried out in an electrolytic bath containing tetrathiomolybdate MoS_4^{2-} anions as the electroactive species. The bath was prepared by mixing aqueous solutions of Na_2S and Na_2MoO_4. It is well known that the formation of thiomolybdates from MoO_4^{2-} proceeds via successive replacement of oxygen and there are five different species of thiomolybdates in the solution at equilibrium: MoO_4^{2-}, $MoO_2S_2^{2-}$, MoO_3S^{2-}, $MoOS_3^{2-}$ and MoS_4^{2-} [16]. Therefore, the preparation of an aqueous thiomolybdate solution requires careful control of reactants concentration and pH. The formation of tetrathiomolybdate proceeds according to the following reaction:

$$MoO_4^{2-} + 4H_2S \Delta MoS_4^{2-} + 4H_2O. \quad (1)$$

In addition to thiomolybdate, such species as K^+, Na^+, $H_2PO_4^-$, HPO_4^{2-}, HS^- and H_2S are also present in the solution. Some of these are involved in equilibrium reactions, such as,

$$H_2PO_4^- \Delta HPO_4^{2-} + H^+, \quad (2)$$

and

$$H_2S \Delta HS^- + H^+. \quad (3)$$

This complicates the process. Nevertheless, it is possible to outline a few guidelines for the preparation of thiomolybdate solutions [16]. Tetrathiomolybdate formation in aqueous media requires a high [S]-to-[Mo] ratio. High sulfide concentrations facilitate the $MoOS_3^{2-}$ to MoS_4^{2-} reaction. The rate constants (for thiomolybdate formation as well as hydrolysis) increase with the basicity of the solution. For all the abovementioned reasons and on the basis of experimental data recently obtained [3–5], the optimal concentration ratio of [Na_2S] to [Na_2MoO_4] was taken as 6:1. The total concentration of sodium sulfide was 0.2 M. The pH of the solution for deposition of MOSC was maintained between 8.0 and 9.5 by KH_2PO_4/K_2HPO_4 buffer. It is also worth noting that high concentrations (0.3 M and higher) of Na_2S require large amounts of KH_2PO_4 for its neutralization and therefore is not practical. Furthermore, lowering the pH of the solution to ≤7 gives rise to MoS_3 and sometimes to MoS_2 precipitation according to the reactions [17]:

$$MoS_4^{2-} + 2H^+ \rightarrow MoS_3 + H_2S, \quad (4)$$

$$MoS_4^{2-} + 2H^+ \rightarrow MoS_2 + H_2S + S. \quad (5)$$

A JSM-6300 scanning microscope (Jeol Co.) equipped with a Link elemental analyzer and a silicon detector was used to study the surface morphology of the cathode films. X-ray diffraction data were obtained with the use of a θ–θ

Scintag powder diffractometer equipped with a Cu K_α source and a liquid-nitrogen germanium solid-state detector. X-ray photoelectron spectroscopy (XPS) tests of as-deposited films were performed with a monochromatic Al K_α source (1,486.6 eV) in ultra-high vacuum (2.5×10^{-10} torr) with a 5600 Multi-Technique System (Physical Electronics, USA). Depth profiles were obtained by argon ion sputtering, at a sputtering rate of 0.5 nm/min based on a SiO_2/Si sample. TOF SIMS tests were conducted with the use of TRIFT II (Physical Electronics USA) under the following operating conditions: primary ions—In^+ and a DC sputtering rate of 2 Å/s based on SiO_2.

Results and discussion

Electrodeposition at constant potential is a very good method for producing thin-film cathodes. The advantage of this method lies in the fact that both the chemical composition and the morphology of the cathode can be controlled by varying the potential of the working electrode.

It was found that electrodeposition of an molybdenum oxysulfide cathode (MOSC) does not occur at potentials less negative than −1.0 V vs Ag/AgCl (3M). Hence, the potentiostatic deposition was carried out at potentials of −1.1, −1.2 and −1.3 V. Generally speaking, electrodeposition of MOSC from a thiomolybdate solution can be represented by the following electrochemical reactions:

$$MoO_xS_{4-x}^{2-} + 2H_2O + 2e^- \rightarrow MoO_xS_{2-x} + 2HS^- + \text{where x can be } 0, 1, 2 \quad (6)$$

$$MoO_xS_{4-x}^{2-} + 2H_2O + 2e^- \rightarrow MoO_{x-1}S_{3-x} + HS^- + \text{where } x \text{ can be } 1, 2, 3 \quad (7)$$

$$MoO_xS_{4-x}^{2-} + 2H_2O + 2e^- \rightarrow MoO_{x-2}S_{4-x} + 4OH^- \quad \text{where } x \text{ can be } 2, 3, 4 \quad (8)$$

It is most likely that the reduction in thiomolybdate happens through cleavage of the Mo–S bond rather than Mo–O, as the Mo–O bond is stronger than Mo–S [17]. Nevertheless, the possibility of reactions occurring via Mo–O bond cleavage cannot be entirely ruled out.

SEM characterization of the deposited molybdenum oxysulfide cathodes

The SEM images of thin cathodes electrodeposited for 15 min are shown in Fig. 1. It is clear that the morphology of electrodeposited cathodes is strongly influenced by the deposition potential. All the samples contain a network of fractured segments and cracks. It is most likely that this happens as a result of internal stresses created during electrodeposition. More prolonged deposition can even cause complete peeling of the cathodes. Another interesting feature is the complex structure of the fractured segments, which consist of many spherical micrograins. These micrograins grow laterally during electrodeposition and coalesce into segments that collapse because of high internal stresses. The size of the segments and the crack width are larger in samples deposited at −1.1 V. Increasing the potential by 100–200 mV drastically changes the morphology of the electrodeposited films—the electrode surface, in addition, is covered by an interconnected granular network. The average size of the granule is about 1 μm. It seems likely that formation of the granular network occurs at potentials above −1.2 V.

It is worth noting that the granular network does not fully cover the electrodeposited layer; this can be attributed to vigorous hydrogen evolution and low current effectiveness. The granular network structure may present a problem in microbattery fabrication, since its microsize structure could penetrate the membrane layer and cause a short-circuit of the microbattery. In view of such undesirable side-effects, the electrodeposition of MOSC should be carried out at cathode potentials lower than −1.2 V and higher than −1.0 V.

The morphology of galvanostatically deposited MOSC under different operating conditions such as current density, deposition time and temperature is shown in the high-resolution SEM micrographs in Fig. 2. According to Fig. 2, samples deposited at different current densities have different morphologies. For instance, in the sample deposited at 15 mA/cm^2, the segments and the cracks are about four times as large as those in the sample deposited at 5 mA/cm^2. Higher current density promotes faster segment growth and, in turn, greater internal stresses for the same deposition time. Moreover, it seems likely that higher current density also increases the rate of coalescence of growing nuclei, in contrast to the common behavior of metal deposition in which an increase in current density usually leads to a decrease in the size of crystallites [18]. Similar enlargement of segments and cracks was observed in the samples deposited for 10 min at different temperature. For sample deposited at 50 °C this effect is even more pronounced than at ambient temperature. It is worth noting that on the sub-micron as well as on the nanometric scale, all deposits are compact, uniform and homogeneous, regardless of the deposition parameters. It was found that the size of the fractured segments and the size of the cracks increase with the deposition time. We believe that the growth of MOSC occurs by the enlargement of 2D clusters, which, in turn, are

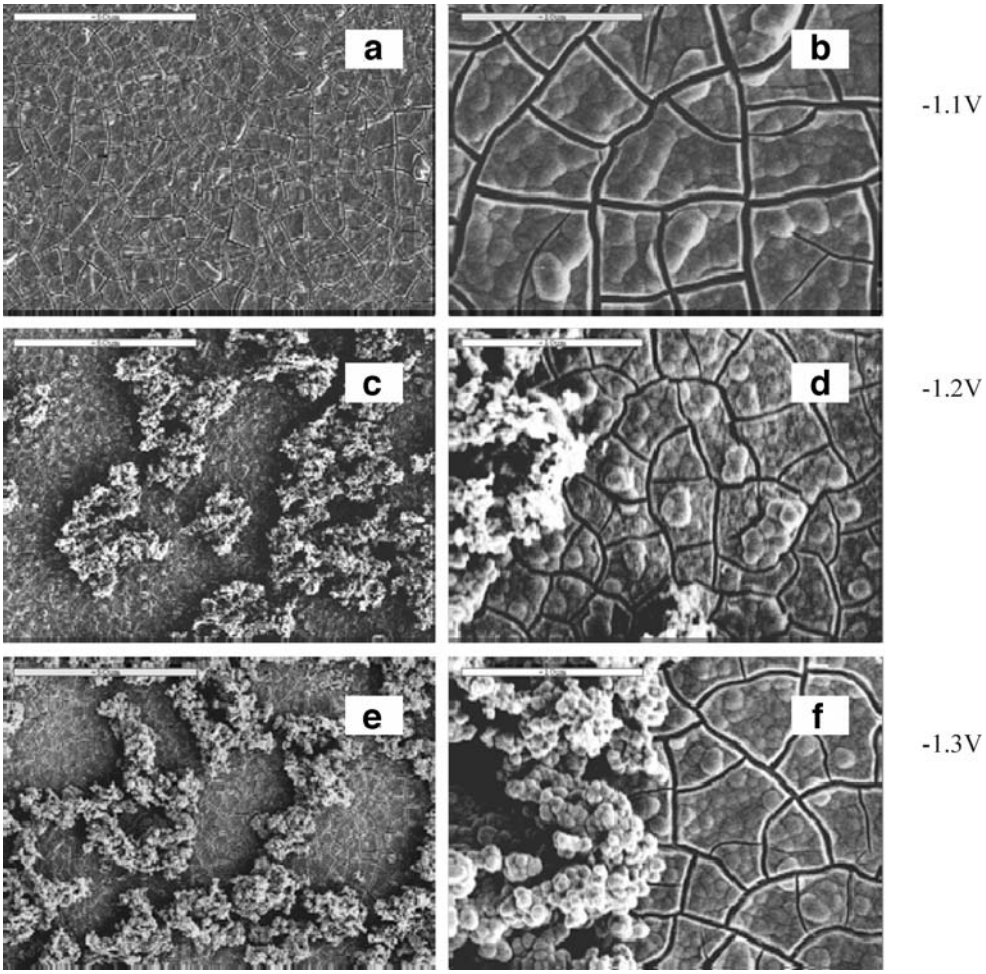

Fig. 1 SEM micrographs of molybdenum oxysulfide cathode electrodeposited at: **a** and **b** −1.1 V, **c** and **d** −1.2 V, **e** and **f** −1.3 V vs Ag/AgCl

formed by the coalescence of primary nuclei. This 2D enlargement is accompanied by the continuous formation of new nuclei, which are growing on already deposited film, forming a new layer for further growth. Such a phenomenon is known as a multinuclear–multilayer mechanism [19] and is probably responsible for MOSC growth both in the galvanostatic and potentiostatic deposition modes.

All electrodeposited films were X-ray transparent, regardless of the deposition conditions. The featureless curves are typical of amorphous materials. It should be mentioned, however, that the crystallites might be too small to give rise to detectable X-ray-diffraction peaks.

TOF-SIMS analysis of electrodeposited MOSCs

TOF-SIMS analysis is the tool of choice for evaluating the chemical composition of thin-film surfaces as well as bulk media. Four different, planar samples deposited in unbuffered solution at various current densities, times and temperatures, namely: 5–5–25 (5 mA/cm^2, 5 min., 25 °C), 5–10–25, 5–10–50 and 15–5–25 were tested by TOF-SIMS.

The negative-ion mass-spectrum of MOSCs spectra were typically recorded during 16 min of sputtering from an area of 50×50 μm. A variety of oxygen- and sulfur-containing molybdenum fragments, like MoO_2, MoS, MoS_2, MoO_3 were found in the cathode. A distinctive feature of the spectra is the presence of polyion clusters containing both oxygen and sulfur, like MoOS, MoO_2S and MoS_2O. These species were found both on the surface and in the bulk of the electrode and, in our opinion, are of primary importance, as their appearance unambiguously indicates formation of molybdenum oxysulfide during electrodeposition [4]. The complete list of molecular fragments is given in Table 1.

TOF-SIMS imaging of sputtered and as-deposited sample 15-5-RT was carried out in order to visualize differences in sulfur and oxygen concentrations on the surface and in the bulk. The ion images of sulfur and oxygen fragments before and after sputtering are shown in Fig. 3. As in the case of SEM micrographs, the ion images reveal fractured segments of deposited material with micron-sized microcracks. The dark and bright regions are those with low and high

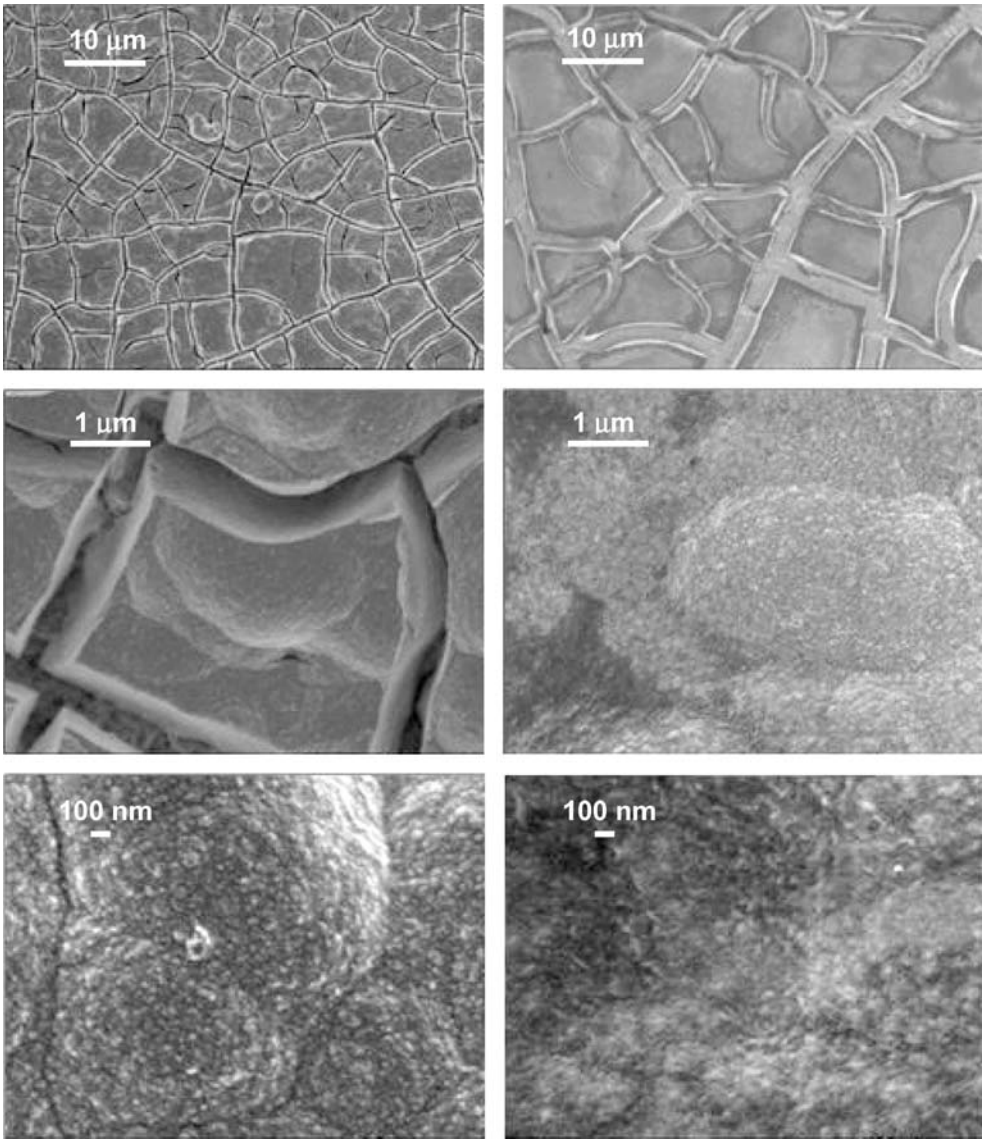

Fig. 2 High-resolution SEM micrographs of cathodes after 5 min of galvanostatic deposition at: 5 mA/cm^2 (*left column*) and 15 mA/cm^2 (*right column*)

concentrations, respectively. Obviously, the images of unsputtered sample show high oxygen concentration along with very low sulfur content, but after 16 min of sputtering, the whole picture is reversed, and there are more bright sulfur than oxygen regions. The sulfur-to-oxygen ratio in the bulk of the deposit is about 1.76 and does not seem to depend much on the electrodeposition parameters.

Figure 4 shows the concentration distribution of fragments for different sputtering time. After 1 min of sputtering, samples 5–10–50 and 15–5–25 show 25–40% higher MoO_3 concentration and lower concentrations of sulfur-containing fragments than do the 5–10–25 and 5–5–25 samples. However, in all the samples, the concentration of MoO_3 is still high, a fact that indicates a highly oxidized surface.

After sputtering for 3, 7 and 16 min, the MoO_3 content in 5–10–50 and 15–5–25 decreases significantly, whereas in samples 5–5–25 and 5–10–25, it shows almost no change. Furthermore, concerning the second major fragment, MoO_2S, it can been seen that its concentration changes drastically during sputtering in samples 5–10–50 and 15–5–25, from about 10% after 1 min up to more than

Table 1 Molecular fragments detected by TOF analyzer in sputtered MOSCs

Molecular fragments			
Most probable (deviation<10%)		Less probable (deviation≥10%)	
MoS	MoO_2	–	–
MoOS	MoO_3	–	–
MoO_2S	MoS_2	MoO_4	–
MoO_3S	$MoOS_2$	MoO_5	–
MoO_2S_2	MoS_3	MoO_4S	MoO_6

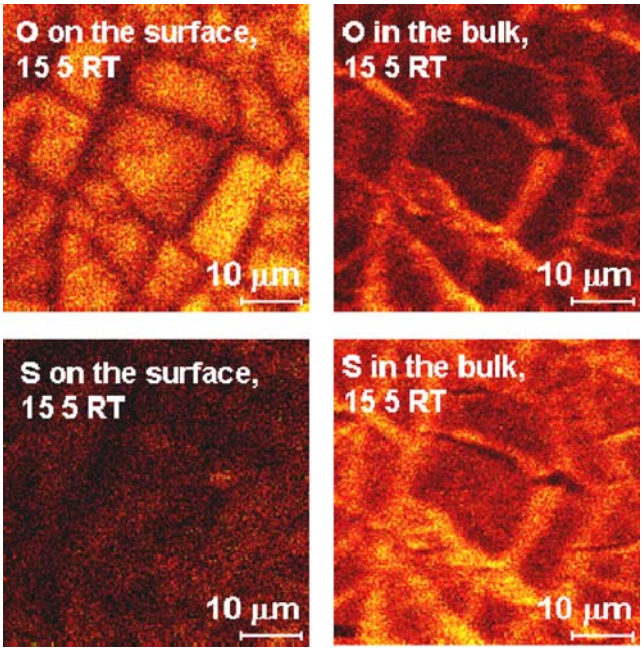

Fig. 3 Ion imaging of 15–5–25 sample on the surface and in the bulk

20% after 16 min of sputtering. At the same time, the MoO_2S concentration in samples 5–5–25 and 5–10–25 does not change by more than 5% after 16 min of sputtering. A sharp decrease in oxygen content in MoO_xS_y fragments upon completion of the sputtering is in agreement with a previous finding of higher sulfur concentration in the bulk in comparison to oxygen. It is noteworthy that the concentration distribution of molybdenum oxysulfide fragments is similar in all the samples, except for 5–5–25. This can be associated with the thickness of the cathode. Indeed, the higher the deposition current, temperature and deposition time, the thicker and fractured the cathode and the more oxidized it is.

According to TOF-SIMS ion images (not shown here), the MoO_xS_y fragments are distributed homogeneously through the deposit at least at sub-micron level. It seems likely that these fragments originated from a submicron-sized single mixed phase rather than from a mixture of various submicron phases.

To check the cathode composition in the crack, TOF-SIMS analysis of six dominant ^{96}Mo-containing fragments was made for electrodeposited samples 5–5–25 and 15–5–25. Since the crack width is about 1 μ, the mass spectrum was recorded from a small area of 1×1 μm. As seen in Fig. 5, the relative distribution of MoO_xS_y fragments in the crack is very similar in both samples. It should be emphasized that the relative distribution of the fragments resembles that found in the bulk of the MOSC deposits. The presence of MoO_xS_y fragments in the crack indicates that the cracks are covered by a film, a few tens of nanometers thick, with chemical composition similar to that in the bulk of the deposit.

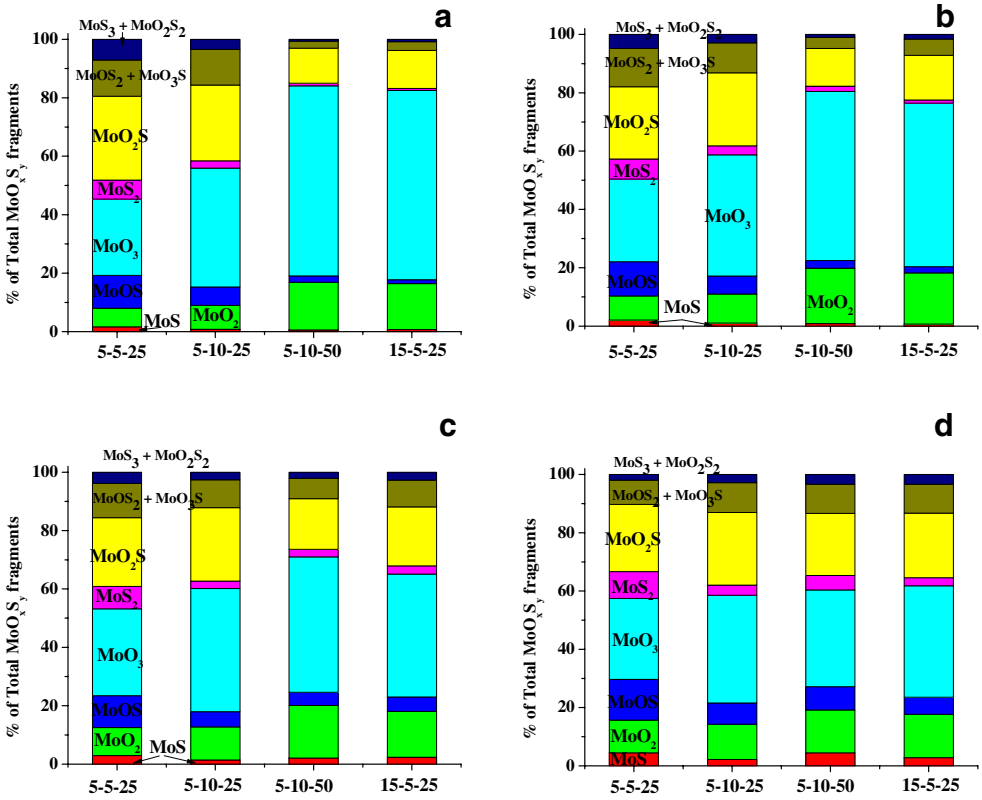

Fig. 4 Molecular fragment concentration distribution after sputtering at: **a** 1 min, **b** 3 min, **c** 7 min and **d** 16 min

XPS analysis of deposited MOSCs at different pH

The Mo 3d, S 2p and O 1s XPS spectra of MOSCs galvanostatically deposited at pH=8.0, 8.5 and 9.5 at 5 mA/cm^2 and 25 °C are shown in Fig. 6. For the sake of convenience, samples deposited at different pH are named ph80, ph85 and ph95, respectively. As seen from the figure, the surface Mo 3d spectra of all the samples consist of two major doublets. The first doublet reflects both Mo(IV)–S and Mo(IV)–O bonds and hence cannot be properly resolved, but the second pair of peaks clearly corresponds to the Mo(VI)–O bond, which can be in MoO_3 or non-stoichiometric MoO_{2+x} compounds. The higher intensity of this doublet in ph95 suggests that its surface is more oxidized than those of the other samples. The S 2p surface spectra of all the samples reveal one broad doublet around 162 eV, which corresponds to the mixed-valence bond Mo–S. The spectrum of pure MoS_2 clearly shows one well-resolved doublet, whereas the spectrum of MoS_3 shows only one broad peak slightly shifted towards higher binding energy (not shown here). Thus, the doublet in the spectra of the MOSCs may actually represent Mo(IV)–S, Mo(VI)–S or even Mo(V)–S bonds. An additional doublet around 168 eV appears in all the samples, but its contribution is significant only in sample ph95. This overlapped doublet represents the S–O bond and is characteristic of impurities on the surface. This doublet disappears after sputtering. Further surface analysis reveals overlapped peaks in the O 1s spectrum, consisting of spectral curves at 530.7 and 532.3 eV.

The former characterizes the Mo–O bond, whereas the latter corresponds to impurities containing S–O bonds. As for the S 2p spectra, the higher binding-energy peak disappears after sputtering. After 6 min of sputtering, there is a slight shift of the Mo 3d peaks towards lower binding energy. This can be related to the sputtering itself, which may partially reduce the analyzed sample. It seems likely that sputtering completely eliminates MoO_3, since its doublet is absent from all spectra. Furthermore, comparison of the bulk spectrum of reference MoO_3 with similar spectra of MOSCs shows no shoulder around 234 eV, which supports the assumption of the existence of a very thin oxidized layer of MoO_3 in all the electrodeposited samples.

On subsequent sputtering of up to 16 min, there is a further shift of the Mo 3d binding energy by 0.1–0.2 eV. The bulk spectra of S 2p are similar regardless of sputtering time and pH. These spectra exhibit one broad peak at 162 eV. It is interesting that no S–O binding-electron doublet was observed in the sputtered samples. The inability to see a well-resolved doublet of the S 2p binding electron implies the presence of mixed-valence Mo–S overlapped doublets.

The XPS analysis of the O 1s binding energy region in sputtered samples reveals one peak for each of samples ph80, ph85 and ph95 that corresponds to the binding energy of the Mo–O bond. Obviously, the highest O 1s binding energy corresponds to the sample prepared at highest pH. As with the bulk spectra of Mo and S, the peak assigned to impurities on the surface disappears after sputtering.

Valuable information regarding the chemical composition of deposited samples can be gained by analyzing the depth-profile graphs in Fig. 7a. After 2 min of sputtering, the concentration of Mo increases two- and threefold and approaches 44.2, 40.9 and 39.1% after sputtering for 16 min. Contrary to molybdenum, the concentration of oxygen is higher at the surface. After 16 min of sputtering, the oxygen concentration decreases sharply to 20.1, 18.2 and 34% for samples ph80, ph85 and ph95, respectively. The sulfur concentration on the surface as well as in the bulk of samples ph80 and ph85 slightly increases from 32.6 to 35.7% and from 34.3 to 38.0%, respectively, whereas in sample ph95, there is a drastic change from 13.45 to 27.0% after 16 min of sputtering. Hence, among the three samples, sample ph95 can be considered an exception because of its highly oxidized surface and high oxygen content along with lower sulfur concentration in the bulk.

Three additional samples were potentiostatically deposited for 10 min at −1.1 V vs Ag/AgCl at pH=8.0, 8.5 and 9.5 and analyzed by XPS. The depth-profile charts are shown in Fig. 7b. As can be seen, the surface is highly oxidized in all the samples with relatively low Mo content. However, the Mo concentration increases rapidly (even after 2 min) and approaches 44.9, 40.8 and 42.1% after 16 min of sputtering. Similarly, the sulfur concentration on the surface is low but it increases up to an almost constant

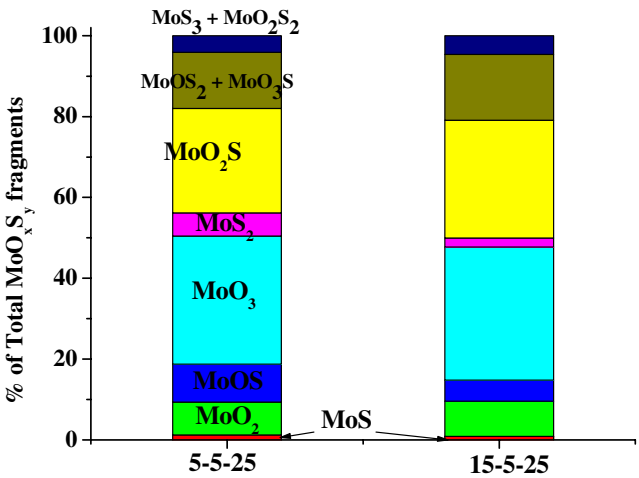

Fig. 5 Distribution of molecular-fragment concentration in the 1×1 μm crack of 1×1 μm

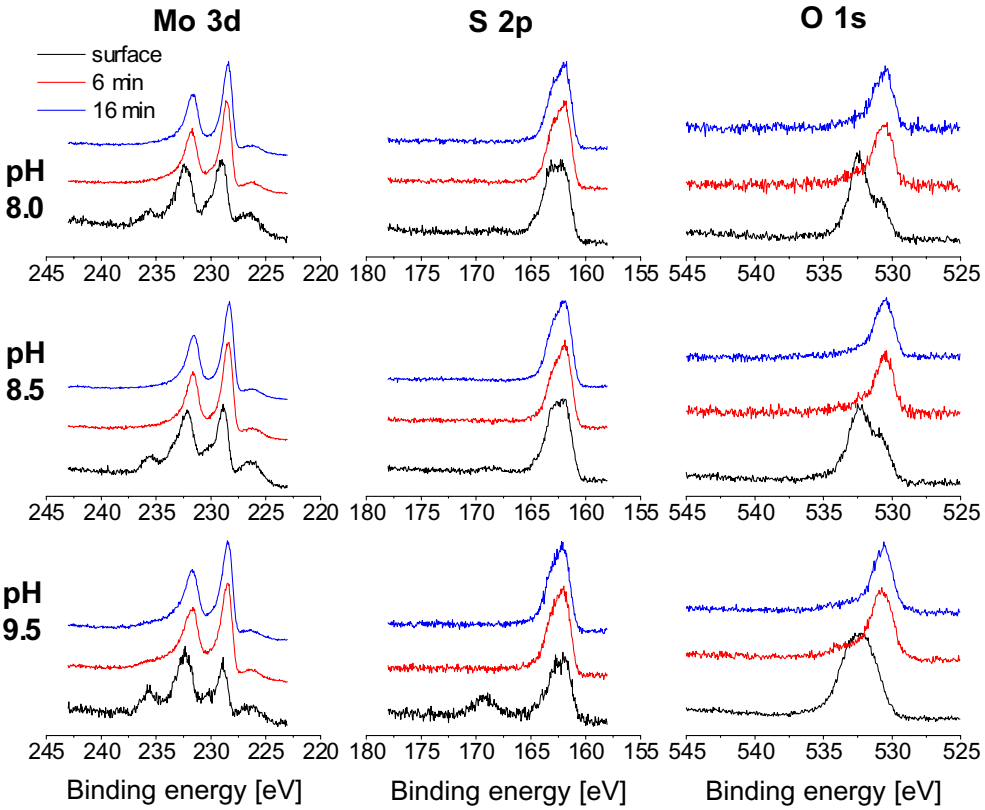

Fig. 6 XPS spectra of molybdenum oxysulfide cathodes deposited for 5 min at 10 mA/cm^2 at different pH=8.0 (*top*), 8.5 and 9.5 (*bottom*), samples ph80, ph85 and ph95

value of 40.2, 38.5 and 33.2% for ph80, ph85 and ph95, respectively. The oxygen profile shows the highest surface concentration of all the analyzed elements—70.5, 57.8 and 74.4%, but it drops sharply to 14.8, 20.6 and 24.6% after 16 min of sputtering. The lowest oxygen and highest sulfur concentrations are found in the sample prepared at the lowest pH (8.0). Correspondingly, the lowest sulfur and highest oxygen concentrations are found in the sample prepared at the highest pH (9.5).

XPS analysis of deposited MOSCs at various current densities and stored under different conditions

Two sets of samples were deposited, one for 10 min at 5 mA/cm^2 and the second for 5 min at 25 mA/cm^2 at pH=8 in unbuffered solutions. The samples were stored under air or in a glove box under argon for several weeks. In accordance with the preparation and storage conditions, the samples were named 5–10-arg, 25–5-arg, 5–10-air and 25–5-air.

Figure 8 shows the main atomic-concentration profiles of the elements as a function of sputtering time. The surface concentration of oxygen is about 70–75% for all the samples. The molybdenum concentration is about 20% for samples deposited at low current density and only 13% for those obtained at 25 mA/cm^2.

The atomic concentration of molybdenum increases on sputtering and approaches 40% after 8 min for samples 5–10-arg, 25–5-arg and 5–10-air. The concentration of O decreases sharply after 4 min of sputtering and reaches 30 and 40% for the argon-stored samples. For the air-stored cathodes, even after 8 min of sputtering, the oxygen concentration is about 50% or more. The higher the deposition rate, the higher the oxygen content. Sulfur atomic-concentration profiles are similar for both argon-stored samples with the bulk concentration about 20%. For the air-stored samples the bulk concentration of sulfur does not exceed 15%.

Chemical composition of MOSCs based on XPS results

As shown above, the conditions of both deposition and storage influence the composition of the thin-film molybdenum oxysulfide cathodes. Table 2 summarizes the change in chemical composition of the cathodes calculated from the XPS depth-profile plots. The bulk stoichiometry of deposited MOSCs was calculated from the atomic concentrations of Mo, S and O at the end of the sputtering. As seen from the table, for almost all the samples, except those deposited at high current density, the relative oxygen content is lower than unity. The relative stoichiometric concentration of sulfur varies from 0.2 to 0.9. The lower

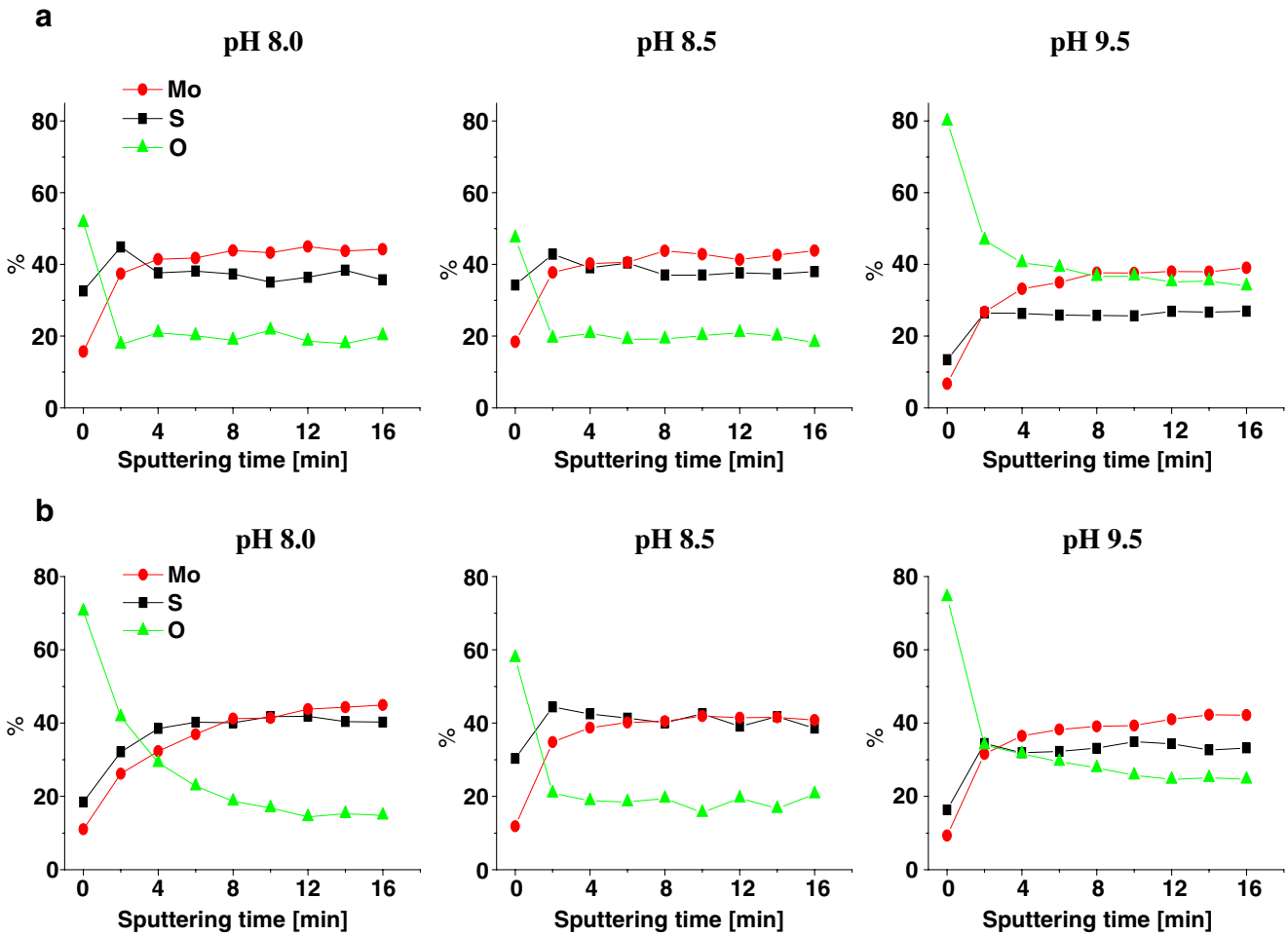

Fig. 7 **a** Depth profiles of galvanostatically deposited ph80, ph85 and ph95 samples (*left to right*). **b** Depth profiles of potentiostatically deposited ph80, ph85 and ph95 samples (*left to right*)

values were detected in cathodes deposited at high current density or stored under air.

The reduction in thiomolybdates results in the formation of MOSCs with the lowest detected oxidation state (+4) for molybdenum [20]. Therefore, the possible stoichiometry of thin MOSCs should be a mixture of $Mo(IV)O_1S_1$, $Mo(V)O_1S_{1.5}$ and $Mo(V)O_{1.5}S_1$, i.e. MoO_xS_y, where $x,y \geq 1$. However, no sample among those stored under argon exhibits such bulk stoichiometry. After sputtering, the atomic concentration of molybdenum is typically higher than that of sulfur. This results from a preferential sputtering process, which removes the more volatile components of the compound, like S and O, and enriches the surface in molybdenum, the lower-sputter-yield species. The low-yield component will accumulate on the sample surface, and its contribution to the sputtered-particle flux will increase until steady-state sputtering will be achieved [21]. It is worth noting that the sputtering of most metal oxides results in a preferential loss of surface oxygen and sometimes a concomitant reduction of the metal to a lower oxidation state [22]. The same phenomenon of preferential sputtering occurs in metal-sulfide and other metal-chalcogenide compounds [23]. In light of the above, it may be seen that the stoichiometry of MOSCs calculated from depth profiles cannot be considered valid. However, by assuming similar behavior during sputtering of all electrodeposited MoO_xS_y cathodes, some conclusions can be drawn regarding the correlation of the real chemical composition of the samples and various preparation and storage conditions. The conclusions are as follows:

- Electrodeposition in unbuffered solutions (pH is poorly controlled) produces high-oxygen and low-sulfur deposits as compared with cathodes deposited in buffered solutions.
- Higher current density results in higher bulk oxygen concentration in the deposit. Potentiostatic deposition results in deposits with slightly higher sulfur and lower oxygen content than does galvanostatic deposition at the same pH.

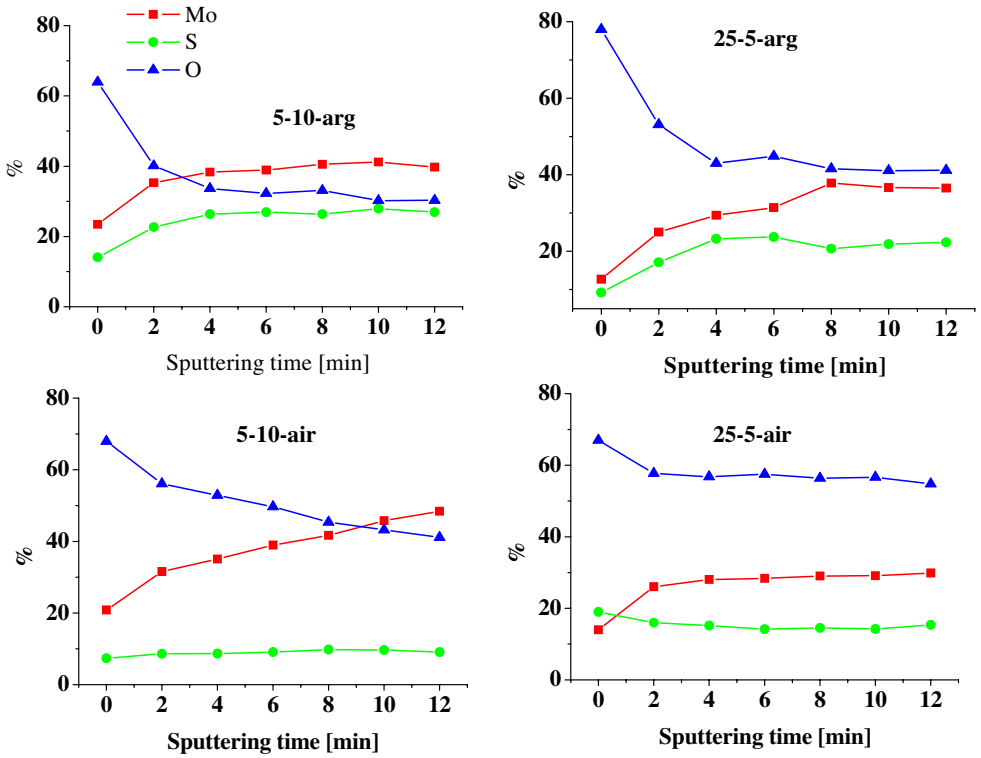

Fig. 8 Depth profiles of 5–10-arg, 25–5-arg, 5–10-air and 25–5-air samples

- Raising the pH from 8 to 9.5 in electrolyte solutions slightly reduces the sulfur content but appreciably increases the oxygen concentration, especially in galvanostatically deposited samples.
- The conditions of storage of electrodeposited samples is of great importance because of the oxidation of deposited material on the surface as well as in the bulk.

The strong dependence of the oxygen content of the deposits on pH and current density is due to the increase in local pH in the near-electrode area. This phenomenon is observed even in buffered solutions. The pH rises when H_2 is evolved simultaneously with the deposition of MOSCs. In addition, it was found that in the absence of buffer in the electrolyte, the oxygen content of the deposited cathodes strongly increases with increasing applied current density (see Table 2). This can be explained by the surface precipitation and occlusion of hydroxides in the growing deposit resulting from an increase in the pH of solution adjacent to the cathode. A near-electrode pH rise decreases the near-electrode concentration of H_2S which, in turn, shifts chemical equilibrium of the reaction (9) to the left, thereby increasing the local concentration of thiomolybdates with higher oxygen content.

$$MoO_xS_{4-x}^{2-} + H_2S \,\Delta\, MoO_{x-1}S_{5-x}^{2-} + H_2O, \qquad (9)$$

This influences the reduction in different thiomolybdate species and the structure, the composition and performance of molybdenum oxysulfide Li and Li–ion batteries.

Table 2 Bulk chemical composition of various deposited MOSCs

Stoich	Deposition	Time	pH	Storage	Mo %	S %	O %
$MoO_{0.8}S_{0.2}$	5 mA/cm^2	10 min	8, unbuf	air	48.4	9.1	41.1
$MoO_{1.8}S_{0.5}$	25 mA/cm^2	5 min	8, unbuf	air	29.9	15.4	54.8
$MoO_{0.8}S_{0.7}$	5 mA/cm^2	10 min	8, unbuf	argon	39.7	26.9	30.3
$MoO_{1.1}S_{0.6}$	25 mA/cm^2	5 min	8, unbuf	argon	36.5	22.3	41.2
$MoO_{0.4}S_{0.8}$	10 mA/cm^2	5 min	8.0, buf	argon	44.2	35.7	20.1
$MoO_{0.4}S_{0.9}$	10 mA/cm^2	5 min	8.5, buf	argon	43.82	38.0	18.2
$MoO_{0.9}S_{0.7}$	10 mA/cm^2	5 min	9.5, buf	argon	39.07	26.9	34.0
$MoO_{0.3}S_{0.9}$	−1.1 V	10 min	8.0, buf	argon	44.92	40.2	14.8
$MoO_{0.5}S_{0.9}$	−1.1 V	10 min	8.5, buf	argon	40.80	38.5	20.6
$MoO_{0.6}S_{0.8}$	−1.1 V	10 min	9.5, buf	argon	42.15	33.2	24.6

Table 3 Calculated MoS_x stoichiometry based on XPS spectra and depth profiles

MoS_x	Linear fit	Deposition	Time	pH
$MoS_{1.23}$	$y=2.13x-140.74$	10 mA/cm^2	5 min	8.0
$MoS_{1.19}$	$y=0.65x-42.01$	10 mA/cm^2	5 min	8.5
$MoS_{0.95}$	$y=0.36x-22.94$	10 mA/cm^2	5 min	9.5
$MoS_{1.30}$	$y=1.21x-79.27$	−1.1 V	10 min	8.0
$MoS_{1.20}$	$y=0.95x-62.10$	−1.1 V	10 min	8.5
$MoS_{1.00}$	$y=0.47x-30.80$	−1.1 V	10 min	9.5

Although it is impossible to establish the exact chemical composition on the basis of the depth profile, (because of preferential sputtering of oxygen and sulfur), the approximate composition of the electrodeposited sample can still be derived. Since there is almost linear correlation between the MoS_x stoichiometry and the Mo $3d_{5/2}$ binding-energy peak, then by plotting the MoS_x composition derived from depth profiles as ordinate against the Mo $3d_{5/2}$ binding energy as abscissa, it is possible to find the basic stoichiometry of MoS_x simply by locating the ordinate whose abscissa equals the surface (unsputtered) value of the binding energy. Using the binding-energy peak difference (Mo $3d_{5/2}$—S $2p_{3/2}$) as the abscissa is favored over the Mo $3d_{5/2}$ peak alone since it serves to reduce errors from charging effects or small drifts in the analyzer electronics [24].

The calculated MoS_x and MoO_xS_y stoichiometries based on XPS spectra and depth profiling are summarized in Tables 3 and 4. It should be emphasized that the calculated stoichiometries are approximate because of errors in the linear fit, which was carried out by way of only two measurement points (at 6 and 16 min of sputtering), as well as the error of ±0.1 eV in the exact determination of the binding energy. In addition, regarding the Mo $3d_{5/2}$ binding-energy peak, the implicit assumption was made that it refers to Mo–S alone, whereas, in fact it characterizes both Mo–S and Mo–O bonds. Once the MoS_x stoichiometry is established, the oxygen content can be estimated by the simple multiplication of the average oxygen-to-sulfur concentration ratio (recorded during the sputtering) by the previously calculated sulfur concentration in MoS_x. Here again, it was assumed that the oxygen-to-sulfur concentration ratio averaged over successive sputtering times could represent the real oxygen-to-sulfur ratio in the bulk of the electrodeposited samples. As indicated in Table 3, as the pH rises, there is an obvious tendency towards increased oxygen and lowered sulfur content in the deposited cathodes. It appears that the deposition regime has little influence on the sulfur concentration and moderate influence on the oxygen concentration in the bulk. Thus, although the stoichiometry after sputtering is not useful for determining chemical composition, it still provides valuable information about the general tendency when one sample is compared with another. On the other hand, the calculated stoichiometries provide information that is more precise and closer to reality regarding the chemical composition than do the sputtered samples.

Planar Li/MoO_xS_y batteries ran over 500 reversible cycles (Fig. 9). The capacity loss of the batteries with cathodes deposited from unbuffered solutions is close to that of buffered and does not exceed 0.08%/cycle. However, the charge/discharge overpotential of lithium insertion/de-insertion was lower by about 15 mV in the cells with cathodes obtained from buffered solutions. In addition, it was found charge/discharge profiles of these cells do not change upon prolonged cycling, whereas the slope of the curves increases in the cells with cathodes from unbuffered solutions. These observations are consistent with [25] and our previous findings [5] of better electrochemical performance of sulfur-rich molybdenum oxysulfide cathodes.

Table 4 Comparison of sputtered and calculated stoichiometries

Sputtered MoO_xS_y	Calculated MoO_xS_y	Deposition regime	Deposition time	pH
$MoO_{0.4}S_{0.8}$	$MoO_{0.64\pm0.04}S_{1.23}$	10 mA/cm^2	5 min	8.0
$MoO_{0.4}S_{0.9}$	$MoO_{0.61\pm0.02}S_{1.19}$	10 mA/cm^2	5 min	8.5
$MoO_{0.9}S_{0.7}$	$MoO_{1.40\pm0.23}S_{0.95}$	10 mA/cm^2	5 min	9.5
$MoO_{0.3}S_{0.9}$	$MoO_{0.55\pm0.03}S_{1.30}$	−1.1 V	10 min	8.0
$MoO_{0.5}S_{0.9}$	$MoO_{0.54\pm0.02}S_{1.20}$	−1.1 V	10 min	8.5
$MoO_{0.6}S_{0.8}$	$MoO_{0.84\pm0.09}S_{1.00}$	−1.1 V	10 min	9.5

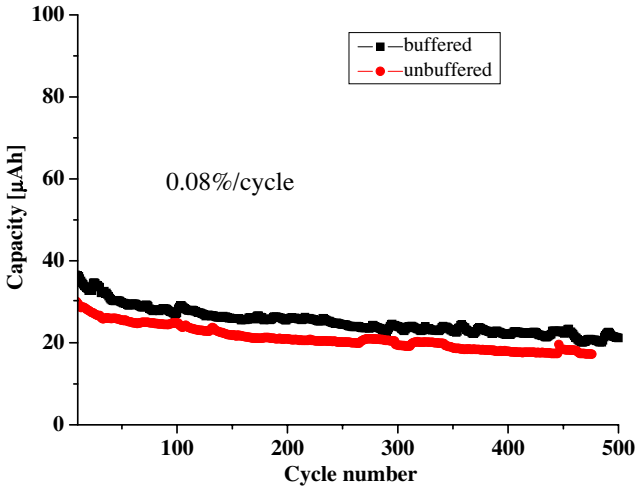

Fig. 9 Plot of capacity vs cycle number of Li/HPE/MoO_xS_y cells

Conclusions

Molybdenum oxysulfide cathodes can be deposited in either the galvanostatic or potentiostatic mode. The deposited cathode always had a network of fractured segments and cracks as a result of internal stresses. The size of both segments and cracks on the planar cathode, deposited at constant current density, increase with increasing current density, deposition time and temperature. All electrodeposited films were X-ray-transparent, regardless of the deposition conditions.

The presence of various molecular fragments of MoO_xS_y (MoOS, MoO_2S etc), both in the surface and bulk TOF mass-spectra of the cathodes indicates that electrodeposition results in the formation of molybdenum oxysulfide films. The high-resolution TOF-SIMS ion images of various MoO_xS_y fragments in the bulk of the deposit indicate that these fragments are distributed homogenously throughout the deposit, at least at the sub-micron level, and most likely originated from a submicron-sized single molybdenum oxysulfide phase, rather than from a mixture of various submicron-sized phases. The concentration of oxygen decreases as a function of depth in the film while that of sulfur increases, until both concentrations attain constant values in all samples. In addition, the sulfur-to-oxygen ratio in the bulk of the deposit is about 1.76 and does not depend much on the electrodeposition parameters. The high-resolution mass spectra of MoO_xS_y fragments inside the cracks show that these cracks are covered by a film a few tens of nanometers thick, of chemical composition similar to that in the bulk of the deposit.

The surface XPS spectra of deposited cathodes revealed the existence of Mo(IV)–O, Mo(VI)–O, Mo(IV)–S and, most likely, Mo(V)–O bonds. These bonds, except for Mo (VI)–O, are also found in the bulk. The sputtering of the samples severely altered the composition of the sample and made impossible the evaluation of both bond type and exact atomic concentration of the elements. However, it was possible to derive the approximate composition of electrodeposited molybdenum oxysulfide samples on the basis of linear correlation between MoS_x stoichiometry and the Mo $3d_{5/2}$ binding-energy peak along with the average oxygen-to-sulfur concentration ratio recorded during the sputtering. It was found that electrodeposition in unbuffered solutions produces deposits with high oxygen and low sulfur content, as compared with cathodes deposited in buffered solutions; higher current density results in higher bulk-oxygen concentration in the deposit; potentiostatic, as compared to galvanostatic deposition, forms deposits with slightly higher sulfur and lower oxygen content at the same pH; an increase in the pH of electrolyte solutions from 8 to 9.5 slightly reduces sulfur content but appreciably increases oxygen concentration, especially in the galvanostatically deposited samples; the storage condition of electrodeposited samples is a matter of great importance because of the oxidation of deposited material on the surface as well as in the bulk.

Acknowledgements We thank Dr. A. Gladkich for carrying out of the TOF-SIMS tests. Financial support of this project has been done by RAMOT -Tel Aviv University Authority for Applied Research and Industrial Development Ltd.

References

1. Nagasubramanian G, Doughty DH (2004) J Power Sources 136:395
2. Nathan M, Haronian D, Peled E, US Patent No. 6197450
3. Nathan M, Golodnitsky D, Yufit V, Strauss E, Ripenbein T, Shechtman I, Menkin S, Peled E (2005) J Microelectromech Syst 14:879
4. Golodnitsky D, Yufit V, Nathan M, Shechtman I, Ripenbein T, Strauss E, Menkin S, Peled E (2006) J Power Sources 153: 281
5. Golodnitsky D, Nathan M, Yufit V, Strauss E, Ripenbein T, Shechtman I, Menkin S, Burstein L, Gladkich A, Peled E (2006) Solid State Ionics 177:2811
6. Yufit V, Nathan M, Golodnitsky G, Peled E (2003) J Power Sources 122:169
7. Whittingham MS (1978) Prog Solid State Chem 12:41
8. Miki Y, Nakazato D, Ikuta H, Uchida T, Wakihara M (1995) J Power Sources 54:508
9. Lince JR, Fleischauer PD (1987) J Mater Res 2:827
10. Imanishi N, Kanamura K, Takehara Z (1992) J Electrochem Soc 139:2082
11. Jacobson AJ, Chianeli RR, Rich SM, Whittingham MS (1979) Mater Res Bull 14:1437
12. Belanger D, Laperriere G, Marsan B (1993) J Electroanal Chem 347:165
13. Auborn JJ, Barberio YL (1987) J Electrochem Soc 134:638
14. Nazri G, Julien C (1992) Solid State Ionics 53–56:400

15. Shembel E, Apostolova R, Nagriny V, Kirsanova I, Grebenkin P, Lytvyn P (2005) J Solid State Electrochem 9:96
16. Clarke NJ, Laurie SH, Blandamer MJ, Burgess J, Hakin A (1987) Inorg Chim Acta 130:79
17. Wang H, Skeldon P, Thompson G, Wood G (1997) J Mater Sci 32:497
18. Kanani N (2004) Electroplatin- basic principles, processes and practice. Elsevier, Kidlington New York Tokyo, pp 170–171
19. Milchev A (2002) Electrolcrystallization: fundamentals of nucleation and growth. Kluwer, New York, pp 189–190
20. Ponomarev EA, Neumann-Spallart M, Hodes G, Levy-Clement C (1996) Thin Solid Films 280:86
21. Werner HW, Boudewijn PR (2002) Depth profiling using sputtering methods. In: Czanderna A, Madey T, Powell C (ed) Methods of surface characterization, vol 5. Beam effects, surface topography, and depth profiling in surface analysis. Kluwer, New York, pp 370–371
22. Malherbe J, Hofmann S, Sanz J (1986) Appl Surf Sci 27:355
23. Bernede J (2001) Appl Surf Sci 171:15
24. Baker M, Gilmore R, Lenardi C, Gissler W (1999) Appl Surf Sci 150:255
25. Schmidt E, Sourisseau C, Meunier G, Levasseur A (1995) Thin Solid Films 260:21